© 2020. Published by The Company of Biologists Ltd | Journal of Cell Science (2020) 133, jcs246785. doi:10.1242/jcs.246785

RESEARCH ARTICLE

Regulation of caveolae through cholesterol-depletion-dependent tubulation mediated by PACSIN2

Aini Gusmira[1,*], Kazuhiro Takemura[2], Shin Yong Lee[1], Takehiko Inaba[1], Kyoko Hanawa-Suetsugu[1,‡], Kayoko Oono-Yakura[1], Kazuma Yasuhara[3], Akio Kitao[2,§] and Shiro Suetsugu[1,§]

ABSTRACT

The membrane-shaping ability of PACSIN2 (also known as syndapin II), which is mediated by its F-BAR domain, has been shown to be essential for caveolar morphogenesis, presumably through the shaping of the caveolar neck. Caveolar membranes contain abundant cholesterol. However, the role of cholesterol in PACSIN2-mediated membrane deformation remains unclear. Here, we show that the binding of PACSIN2 to the membrane can be negatively regulated by cholesterol. We prepared reconstituted membranes based on the lipid composition of caveolae. The reconstituted membrane with cholesterol had a weaker affinity for the F-BAR domain of PACSIN2 than a membrane without cholesterol. Consistent with this, upon depletion of cholesterol from the plasma membrane, PACSIN2 localized at tubules that had caveolin-1 at their tips, suggesting that cholesterol inhibits membrane tubulation mediated by PACSIN2. The tubules induced by PACSIN2 could be representative of an intermediate of caveolae endocytosis. Consistent with this, the removal of caveolae from the plasma membrane upon cholesterol depletion was diminished in the PACSIN2-deficient cells. These data suggest that PACSIN2-mediated caveolae internalization is dependent on the amount of cholesterol, providing a mechanism for cholesterol-dependent regulation of caveolae.

This article has an associated First Person interview with the first author of the paper.

KEY WORDS: F-BAR domain, PACSIN2, Syndapin II, Caveolae, Cholesterol

INTRODUCTION

The Bin-Amphiphysin-Rvs (BAR) domain superfamily of proteins has been shown to play major roles in the shaping of the cell membranes (Daumke et al., 2014; Doherty and McMahon, 2009; Nishimura et al., 2018; Simunovic et al., 2015; Suetsugu et al., 2014). The PACSINs (also known as syndapins) are Fes/CIP4 homology (FCH)-BAR (F-BAR) domain proteins that are localized to invaginations, such as endocytic sites, including caveolae (Hansen et al., 2011; Koch et al., 2012; Seemann et al., 2017; Senju et al., 2011). Structural analysis of the PACSIN2 F-BAR domain has revealed that it has a positively charged concave surface that acts to induce membrane invagination, analogous to what is seen for other BAR and F-BAR domains, and binds to negatively charged lipids, including phosphatidylserine (PS), via electrostatic interaction (Rao et al., 2010; Shimada et al., 2010). The membrane binding of PACSIN2 does not appear to be specifically dependent on particular negatively charged lipids, such as phosphatidylinositol 4-phosphate [PI(4)P] and phosphatidylinositol 4,5-bisphosphate [$PI(4,5)P_2$] (Dharmalingam et al., 2009). The F-BAR domains of PACSINs have specific hydrophobic loops that protrude on the concave membrane-binding surface of the structure, which are inserted into the hydrophobic region of the membrane (Shimada et al., 2010).

The membrane of caveolae is composed of different types of lipids, namely cholesterol and phospholipids (Hubert et al., 2020; Morén et al., 2012; Murata et al., 1995; Ortegren et al., 2004; Schlegel et al., 1999). Cholesterol is highly enriched in caveolae (Ortegren et al., 2004; Razani et al., 2002; Smart et al., 1999). Up to 41% of the membrane lipid content of caveolae in adipocytes is reported as being cholesterol, which is higher than the typical amount of cholesterol found outside caveolae (∼22%) (Ortegren et al., 2004). Furthermore, cholesterol is an essential component of caveolae, because cholesterol depletion impairs the morphology of caveolae (Breen et al., 2012; Dreja et al., 2002; Murata et al., 1995; Parpal et al., 2001; Razani et al., 2002; Smart et al., 1999). Owing to cholesterol enrichment, caveolae are sometimes considered to be subsets of lipid rafts with caveolin protein localization (Patel and Insel, 2009; Pike, 2003; Razani et al., 2002).

Phospholipids are composed of two fatty acids and one hydrophilic group, such as serine, ethanolamine, choline, and inositol. Phospholipids are primarily classified by their hydrophilic group. The major phospholipids that are present in the cellular membrane are phosphatidylethanolamine (PE), phosphatidylcholine (PC), phosphatidylserine (PS) and phosphatidylinositol (PI). PC is widely known to be the most abundant phospholipid in the cell membrane, comprising 41–57 mol% of total glycerophospholipids (van Meer et al., 2008; Yang et al., 2018). PC is also a prominent phospholipid in caveolae (Huot et al., 2010; Pike et al., 2005; Smart et al., 1999), while PS has been found to be abundant in the cytoplasmic leaflet of caveolae (Fairn et al., 2011; Pike et al., 2005). The depletion of PS has been shown to result in the loss of caveolar morphology (Hirama et al., 2017). The main fatty acids of caveolar phospholipids are oleic acid (C18:1), palmitic acid (C16:0) (Cai et al., 2013; Huot et al., 2010) and stearic acid (C18:0) (Cai et al., 2013). 1-Palmitoyl-2-oleoyl (16:0-18:1) PC (POPC) and 1-palmitoyl-2-oleoyl (16:0-18:1) PS (POPS) are the most abundant forms of PC and PS found in the caveolar membrane, respectively (Pike et al., 2005).

The structural proteins of caveolae are considered to be the caveolins (Rothberg et al., 1992), which interact with cholesterol

[1]Division of Biological Science, Nara Institute of Science and Technology, Ikoma, Nara 630-0192, Japan. [2]School of Life Science and Technology, Tokyo Institute of Technology, Meguro, Tokyo 152-8550, Japan. [3]Division of Material Science, Nara Institute of Science and Technology, Ikoma, Nara 630-0192, Japan.
*Present address: Faculty of Pharmacy, Universitas Indonesia, Jawa Barat 16424, Indonesia. ‡Present address: Graduate School of Brain Science, Doshisha University, Kyotanabe, Kyoto 610-0394, Japan.

§Authors for correspondence (akitao@bio.titech.ac.jp; suetsugu@bs.naist.jp)

S.S., 0000-0002-4612-0628

Handling Editor: Tamotsu Yoshimori
Received 26 March 2020; Accepted 24 August 2020

Journal of Cell Science (2020) 133, jcs246785. doi:10.1242/jcs.246785

(Murata et al., 1995) and cavin proteins (Hill et al., 2008). Furthermore, palmitic acid and stearic acid are the predominant fatty acids that bind to caveolin-1 (Cai et al., 2013). A caveola contains ∼150 caveolin proteins (Khater et al., 2019; Pelkmans and Zerial, 2005; Tachikawa et al., 2017), providing a possible explanation for the enrichment of cholesterol in caveolae. PACSIN2 is localized to the neck of caveolae and has been suggested to interact with caveolin-1 through its F-BAR domain (Senju et al., 2011). Approximately 35–48% of endogenous caveolin-1 dots have been found to colocalize with PACSIN2, implying that PACSIN2 is involved in the endocytic function and the formation of a subset of caveolae (Hansen et al., 2011; Senju et al., 2011). The knockdown of PACSIN2 in HeLa cells has been found to impair the morphology of caveolin-1-associated membranes (Hansen et al., 2011; Senju et al., 2011, 2015). Tension applied to the plasma membrane induces the flattening of caveolae (Sinha et al., 2011). Upon the application of tension, PACSIN2 is removed from caveolae through protein kinase C (PKC)-mediated phosphorylation of PACSIN2 (Senju et al., 2015). The PKC-phosphorylated PACSIN2 has a weaker affinity to liposomes made from the total lipid fraction of bovine brain, which has been widely used for the study of BAR domains (Senju et al., 2015; Senju and Suetsugu, 2015).

The above-mentioned studies show that PACSIN2 binds to the membrane via its F-BAR domain. However, the lipid characteristics of caveolae that affect the ability of PACSIN2 to mediate membrane deformation have not yet been studied. Furthermore, the effect of cholesterol has not been specifically studied in the model membranes used in *in vitro* assays, nor has tension been applied to the membranes. Therefore, in this study, we attempted to examine the role of cholesterol and tension on the binding of PACSIN2 to membranes. We investigated the effect of cholesterol on the binding affinity of the PACSIN2 F-BAR domain, and the effect on membrane shaping mediated by PACSIN2 in liposomes composed of phospholipids with the specific fatty acids that are abundant in caveolae, that is POPC and POPS, in the presence or absence of cholesterol and of membrane tension. We found that cholesterol reduced the affinity of the PACSIN2 F-BAR domain for the liposomes, inhibiting the formation of straight membrane tubules. Consistent with this, the depletion of cholesterol from the plasma membrane resulted in enhanced formation of PACSIN2-localized tubules that have caveolin-1. The tubules formed could represent the intermediates of caveolar endocytosis. Results with PACSIN2-knockout cells demonstrated that caveolar removal from the plasma membrane is dependent on PACSIN2. Therefore, this study indicates a novel role of PACSIN2 in the removal of cholesterol-lacking caveolae from the plasma membrane. This might represent an important mechanism for the maintenance of cholesterol-enriched caveolae on the plasma membrane.

RESULTS

Binding of PACSIN2 to liposomes with or without cholesterol

An acute depletion of cholesterol can be achieved by the application of methyl-β-cyclodextrin (MβCD) to cells (Hirama et al., 2017; Ohtani et al., 1989; Puri et al., 2001; Simons and Toomre, 2000; Zidovetzki and Levitan, 2007). Therefore, we tested two membranes, one with and one without cholesterol. To mimic the caveolar lipid membrane, we prepared liposomes using POPC, POPS and cholesterol at a 33, 22 and 45 molar ratio [denoted POPC/POPS/Chol(45)], or by using POPC and POPS at a 60 and 40 molar ratio (denoted POPC/POPS), as discussed above. Membrane packing defects and charge density were thought to to affect the binding of PACSIN2, because of the presence of the hydrophobic loop to be inserted into the membrane and of the positively charged surface (Shimada et al., 2010). To precisely describe the packing defects and charge density in our liposomes, we estimated the packing defects and charge density of the reconstituted membranes using molecular dynamics simulations (Fig. 1A). We estimated the charge densities and the area of the packing defects of >10 Å^2 within the simulated membrane. We also calculated the area of the membrane per lipid mass in order to be able to compare the affinity of PACSIN2 per membrane area. The calculation indicated that the addition of cholesterol decreased the charge density while increasing the packing defects (Fig. 1A).

The effect of cholesterol on the binding affinity of the PACSIN2 F-BAR domain [amino acids (aa) 1–343] was investigated by determining the concentration of liposomes required for 50% binding using a liposome co-sedimentation assay (Fig. 1B). From the amount of the PACSIN2 proteins in the liposomal pellet, we estimated the fraction of PACSIN2 that bound to the membrane. The percentages of the PACSIN2 F-BAR domain that bound to the liposomes in the co-sedimentation assay were plotted as a function of the membrane area and the molar concentration of PS (Fig. 1C, D). The membranes were assumed to be unilamellar for the plots, because the quenching of the small amount of fluorescent lipids that were incorporated into the membrane was ∼50% when the liposomes were intact (Fig. S1). The proportion of the PACSIN2 F-BAR domain binding to the POPC/POPS liposomes reached up to 50% when the total membrane area was 4.3×10^7 μm^2/μl, while binding to POPC/POPS/cholesterol liposomes reached 50% when the total membrane area of was 6.5×10^7 μm^2/μl, suggesting that the presence of cholesterol decreased the affinity of the PACSIN2 F-BAR domain for the membrane (Fig. 1C). Interestingly, when we examined the 50% binding with respect to the DOPS concentration, the binding of the PACSIN2 F-BAR domain to the POPC/POPS liposomes reached 50% when the DOPS concentration was 23 μM in the absence of cholesterol, and at 27 μM in the presence of cholesterol (Fig. 1D). The difference in the concentration for 50% binding was smaller as a function of the PS concentration compared to that of the area. This could be explained by the decrease in the charge density in this condition (Fig. 1A). The increase in the packing defect upon the addition of cholesterol might not contribute to the affinity of PACSIN2 for the membrane; rather, the charge density in the presence of cholesterol may account for the difference in the membrane binding of PACSIN2 in a cholesterol-dependent manner.

Membrane deformation by PACSIN2 is cholesterol dependent

Membrane remodeling is thought to be affected by the affinity of the binding proteins as well as by the bending rigidity of the membrane (Dimova, 2014). The presence of cholesterol, even at 10%, stiffens the membrane (Henriksen et al., 2006, 2004). In order to investigate whether cholesterol influenced the membrane remodeling of PACSIN2, we analyzed the morphology of liposomes in the presence of the PACSIN2 F-BAR domain using transmission electron microscope (TEM). The POPC/POPS liposomes were found to be deformed by the PACSIN2 F-BAR domain into straight tubular shapes (Fig. 1E,F). However, the POPC/POPS/Chol(45) liposomes were remodeled into tubules resembling an assembly of small vesicles (Fig. 1E,G), similar to ‘beads on a string’, which correlates with previous observations in bovine Folch liposomes (Wang et al., 2009). The diameters of all tested liposomes in the absence of the PACSIN2 F-BAR domain were similar to each other (Fig. 1G). These results indicate that cholesterol suppresses the

Journal of Cell Science (2020) 133, jcs246785. doi:10.1242/jcs.246785

A

w/o tension

Components (mol%)	<h> (nm)	Q (e/nm^2)	f_{def}(%)	area (m^2/g)
POPC60, POPS40	4.1±0.042	-0.66±0.008	0.01±0.03	480.5±5.6
POPC33, POPS22, Cholesterol45	4.6±0.028	-0.52±0.004	0.34±0.21	433.1±3.2

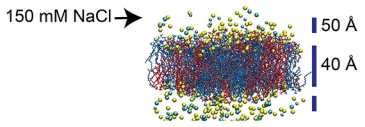

w/ tension

Components (mol%)	<h> (nm)	Q (e/nm^2)	f_{def}(%)	area (m^2/g)
POPC60, POPS40	4.1±0.025 4.1±0.025	-0.66±0.005	0.01±0.03 (150 mM) 0.01±0.03 (230 mM)	478.4±3.3
POPC33, POPS22, Cholesterol45	4.6±0.023 4.6±0.023	-0.52±0.003	0.31±0.19 (150 mM) 0.27±0.17 (230 mM)	433.0±2.2

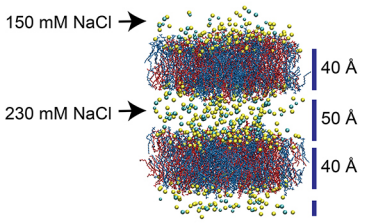

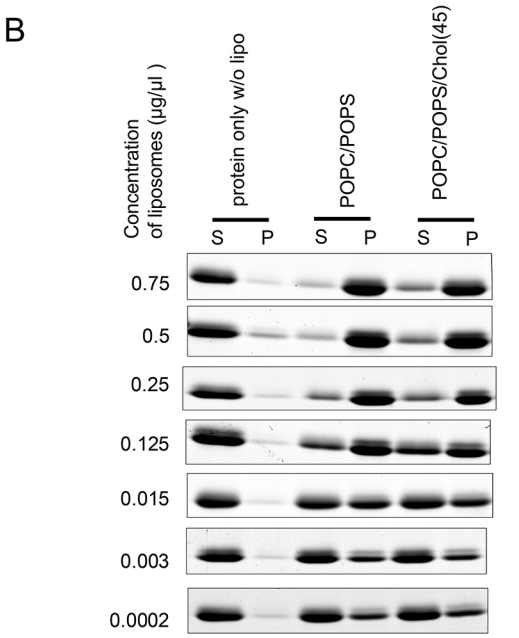

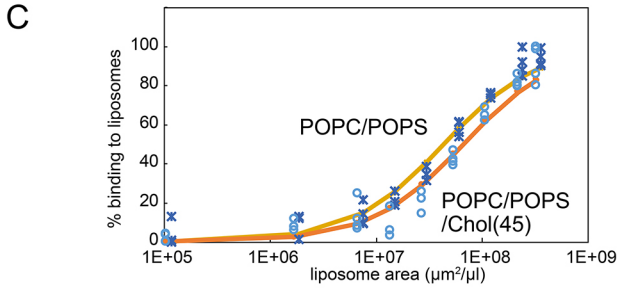

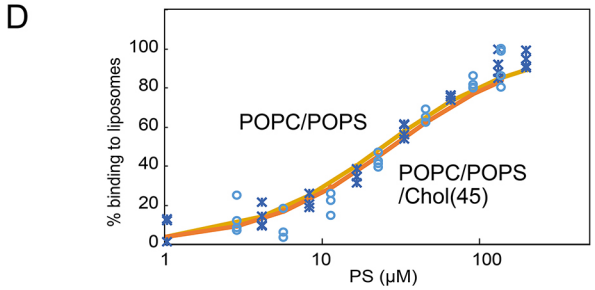

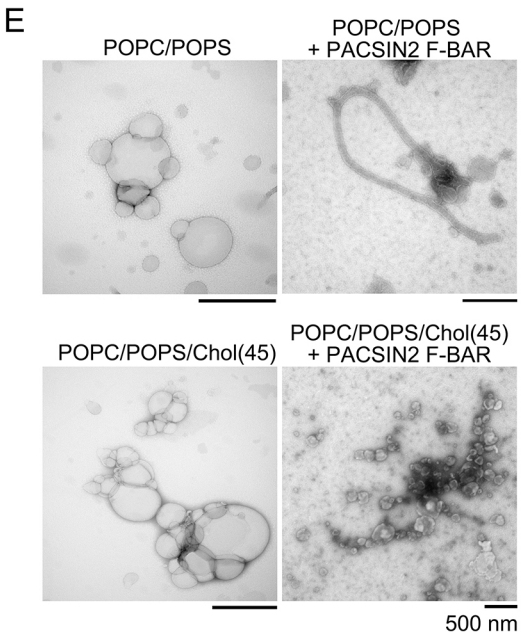

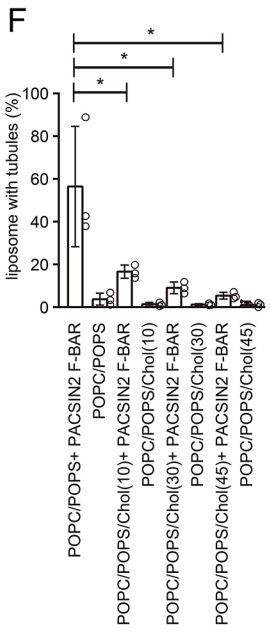

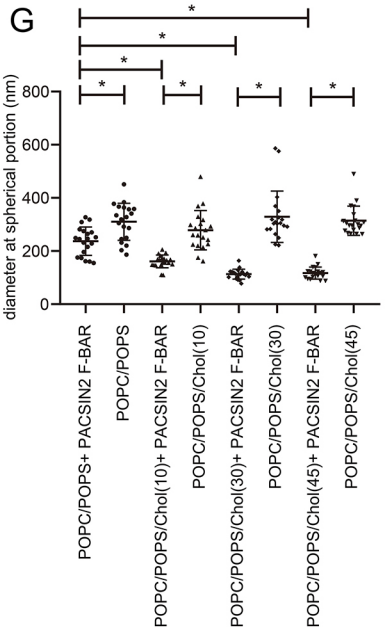

Fig. 1. See next page for legend.

Journal of Cell Science (2020) 133, jcs246785. doi:10.1242/jcs.246785

Fig. 1. Effect of cholesterol on membrane binding of the PACSIN2 F-BAR domain. (A) Molecular dynamics simulation for the estimation of model membrane parameters. The height of the membrane <h> (nm), the charge density (electron/nm^2), the average percentage of packing defects of >10 Å^2 to the total membrane area (f_{def}), and the area of the membrane (m^2/g) are shown in the table. An illustration of the membrane system in the simulation is presented on the right. (B–D) The binding of purified a PACSIN2 F-BAR domain (5 µM) to liposomes comprised of POPC/POPS and POPC/POPS/cholesterol, as determined by liposome co-sedimentation assay. The PACSIN2 F-BAR domain was incubated with liposomes and the supernatant (S) was separated from the pellet (P) after centrifugation. The S and P fractions were subjected to SDS-PAGE and stained using CBB. The binding graph represents the percentage of binding of the PACSIN2 F-BAR domain against the concentration of liposomes. Experiments were performed at least three times at each liposome concentration. The half maximum concentration of the binding was analyzed using Excel solver. *n*=3. (E) Electron microscopy images of negatively stained POPC/POPS or POPC/POPS/cholesterol(45) liposomes in the presence of the PACSIN2 F-BAR domain (5 µM). Liposome concentration was 0.125 and 0.181 µg/µl, respectively, in order to have the same amount of PS in the reaction. (F) Quantification of the proportion (%) of liposomes with tubules when using liposomes composed of POPC/POPS, POPC/POPS/cholesterol(10), POPC/POPS/cholesterol(30) or POPC/POPS/cholesterol(45) in the presence or absence of PACSIN2 as shown in E and Fig. S2A. A circle represents the mean of more than 50 liposomes in each experiment. Three independent experiments were performed. **P*<0.05 (one-way ANOVA followed by Tukey's post hoc test). (G) The distribution of the diameter of liposomes. The diameter of the liposome with tubules was considered to be the spherical portion of the liposomes. More than 20 liposomes were measured. **P*<0.01 (Student's *t*-test). Error bars show the s.d.

formation of straight tubules by the PACSIN2 F-BAR domain, which might play a role in the formation of the caveolar shape.

To confirm the cholesterol-dependent membrane deformation mediated by PACSIN2, we prepared liposomes with various cholesterol concentrations. As the cholesterol concentration increased, the efficiency of the tubule formation mediated by the PACSIN2 F-BAR domain decreased (Fig. 1F). Liposomes with 10% cholesterol [denoted POPC/POPS/Chol(10) liposomes] were tubulated by the PACSIN2 F-BAR domain, but interestingly, the tubules were sometimes not straight and were constricted (Fig. S2A). The liposomes with 30% cholesterol did not exhibit a lot of tubulation, but rather resembled 'beads-on-string' (Fig. S2A). Molecular dynamics simulations suggested that the charge density decreases upon an increase of cholesterol (Fig. 1A; Fig. S2B). However, at 10% cholesterol, no decrease in the charge density was detected by the molecular dynamics simulation as compared with the liposomes without cholesterol (Fig. S2B), suggesting that it is characteristics other than the charge density, such as the bending rigidity of the membrane, also affect PACSIN2-mediated membrane tubulation.

To further confirm the cholesterol dependence of the tubule formation mediated by the PACSIN2 F-BAR domain, we examined the liposomes used in the above experiments, upon treatment with 2 mM MβCD, which is a higher concentration than that of cholesterol in the liposomes. In the 2 mM MβCD condition, we observed similar tubule formation in the POPC/POPS/Chol(45) liposomes to that in POPC/POPS liposomes in the presence of PACSIN2 F-BAR domain (Fig. S2C,D). These data strongly suggest that the PACSIN2-mediated membrane deformation is affected by the cholesterol content of the membrane.

Membrane binding of PACSIN2 is not altered by introduction of hypotonic tension *in vitro*

In our previous study, PACSIN2 was found to respond to membrane tension that was applied through hypotonic osmolarity changes (Senju et al., 2015). PACSIN2 was found to be removed from the caveolae upon hypo-osmotic treatment of the cells, presumably due to a phosphorylation-induced weakening of the membrane binding as a result of the introduction of a negative charge. However, it is possible that the tension, tension-induced packing defects, and tension-induced resistance to deformation might modulate the binding of PACSIN2 to the cell membranes. Here, by applying hypo-osmotic-induced tension, we examined the effect of tension on the binding and remodeling activity of the PACSIN2 F-BAR domain on liposomes. Osmotic pressure induces the stretching of liposomes, which eventually causes liposomes to swell and rupture (Alam Shibly et al., 2016; Finkelstein et al., 1986). We determined the tension threshold at which liposomes could exist without rupturing by observing the leakage of the fluorescent molecules from the liposomes. The liposomes were constructed using buffer containing carboxyfluorescein (CF), and then purified using gel filtration and centrifugation to remove any CF found outside the liposomes. The liposomes were then treated with a hypotonic buffer to induce membrane tension. High hypotonic tension can lead to liposome rupture, followed by leakage of the internal CF, which can be quantified by the spectro-fluorometry analysis of CF released from the liposomes (Hamai et al., 2007; Shoemaker and Vanderlick, 2002). Here, we examined the release of CF from the liposomes made of porcine brain Folch fraction, a total fraction of porcine brain, under several levels of hypotonic tension (Fig. 2A). The CF fluorescence was found to increase as the osmolarity difference increased, suggesting that the rupture of the liposomes increased as the tension increased. Then, we applied the tension through introducing an 160 mOsmol osmolarity difference to the POPC/POPS liposomes and to POPC/POPS/cholesterol liposomes and observed the leakage. The leakage was considered to be similar to that of porcine Folch liposomes (Fig. 2B).

The presence of packing defects upon tension application were also examined by molecular dynamic simulations. The number of ions were adjusted according to the experimental setup above to mimic the 160 mOsmol difference in osmolarity. In these cases, no changes in the packing defects were observed (Fig. 1A). Therefore, the tension does not induce packing defects, and the formation of packing defects upon introduction of membrane tension was considered to be negligible.

Then, we selected the osmolarity inside of the liposomes to be 460 mOsmol, and that of the outside to be 300 mOsmol, to obtain an osmolarity difference of 160 mOsmol. We then examined the binding affinity of the PACSIN2 F-BAR domain to POPC/POPS and POPC/POPS/Chol(45) liposomes under both isotonic and hypotonic tension using a liposome co-sedimentation assay (Fig. 2C). Since the amount of the PACSIN2 proteins in the liposomal pellet was similar independent of tension, the binding affinity of PACSIN2 F-BAR under both isotonic and hypotonic tension appeared to be similar (Fig. 2D), suggesting that the membrane tension below the rupture induction does not alter the amount of the PACSIN2 F-BAR domain on the liposomes.

Acute depletion of cholesterol induces PACSIN2-mediated tubulation in HeLa cells

We next examined whether the amount of cholesterol could modulate the membrane tubules to which PACSIN2 was localized in cells. Overexpression of the PACSIN2 F-BAR domain can induce massive tubulation in cells (Senju et al., 2011). Here, we used HeLa cells overexpressing the GFP–PACSIN2 F-BAR domain, and selected for cells with PACSIN2 F-BAR domain expression but without this massive tubulation. These cells were observed using a microscope during the addition of MβCD to deplete cholesterol from the plasma

Journal of Cell Science (2020) 133, jcs246785. doi:10.1242/jcs.246785

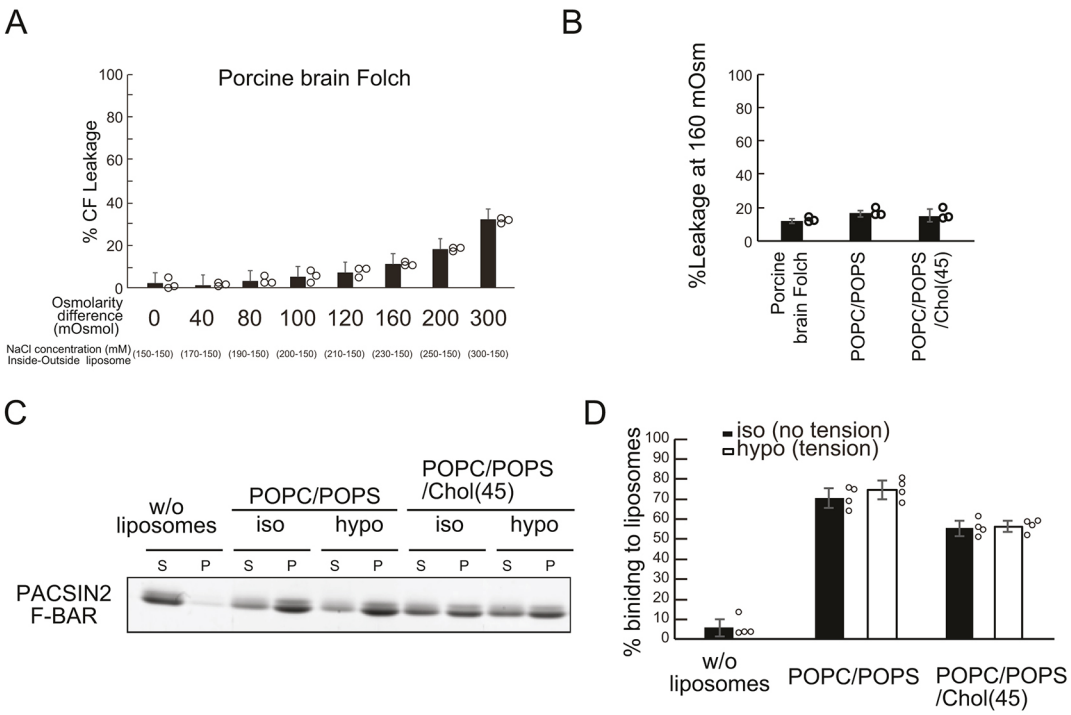

Fig. 2. Osmolality and membrane binding of the PACSIN2 F-BAR domain. (A) The percentage of carboxyfluorescein (CF) released from porcine brain Folch liposomes upon exposure to different levels of tension. (B) The percentage of CF released from several types of liposomes at a tension induced by a 160 mOsmol difference between the inside and outside of the liposomes. Experiments were performed three times. Error bars indicate the s.d. (C) Binding affinity of the PACSIN2 F-BAR domain (5 µM) to POPC/POPS and POPC/POPS/cholesterol under isotonic (iso, no tension) and hypotonic (hypo) tension as determined in a co-sedimentation assay. The PACSIN2 F-BAR domain was incubated with liposomes, and the supernatant (S) was separated from the pellet (P) by centrifugation. S and P fractions were subjected to SDS-PAGE and CBB staining. Liposome concentration was 0.125 µg/µl. w/o, without. Experiments were performed three times. A representative experiment is shown. (D) Quantification of C. The assay was performed four times. Error bars indicate the s.d.

membrane. The depletion of cholesterol induced the acute tubules, with the PACSIN2 F-BAR domain localization (Fig. 3A), which appears to be consistent with the observations of the *in vitro* tubulation with PACSIN2.

Next, we examined the behavior of full-length PACSIN2 and caveolin-1 upon treatment with MβCD. Caveolin-1–GFP and PACSIN2–mCherry were expressed at endogenous protein levels. The tubular localization of PACSIN2 was almost absent without MβCD treatment, which is consistent with the cholesterol-mediated suppression of the tubulation *in vitro* (Fig. S2C,D). These cells were treated with MβCD in 2 mM step-increases up to 10 mM. Upon treatment with 2 mM MβCD, acute tubules of PACSIN2–mCherry were observed, with the tips of the tubules sometimes staining positive for caveolin-1–GFP (Fig. 3B). These tubules were generated from caveolin-1 dots, which were presumed to be caveolae. Consistent with the previous reports, which show that approximately half of the caveolin-1 colocalizes with PACSIN2 (Senju et al., 2011), a proportion of caveolin-1 dots (43±4% from seven cells; mean±s.d.) colocalized with PACSIN2 (Fig. 3C). Furthermore, a proportion of PACSIN2 tubules (33±14%) were observed without detectable levels of caveolin-1 (Fig. 3C), which might suggest that PACSIN2 functions in the structures other than caveolae. These findings suggest that caveolar invaginations become elongated into tubules upon cholesterol depletion in a process that is mediated by PACSIN2. Interestingly, the tubules and caveolin-1 eventually disappeared, suggesting that the caveolin-1 proteins or caveolae were internalized upon cholesterol depletion by MβCD. Therefore, we suggest that PACSIN2 mediates caveolar internalization upon cholesterol depletion via its tubule-forming ability.

PACSIN2-mediated internalization of caveolin-1 upon cholesterol depletion

The amount of caveolae in cells has been shown to be dependent on cholesterol (Hailstones et al., 1998). However, the mechanism for cholesterol-dependent caveolar regulation is unknown. We made PACSIN2-knockout cells using CRISPR/Cas9 techniques and determined the levels of caveolin-1 upon depletion of cholesterol with different concentrations of MβCD. The cells were seeded in serum-free medium and treated with MβCD for 3 h. After MβCD treatment, the amount of caveolin-1 relative to GAPDH was found to be decreased in the parental HeLa cells; however, the amount of caveolin-1 was increased in PACSIN2-knockout cells compared with that in the parental HeLa cells (Fig. 4A,B). The decrease of caveolin-1 in the parental HeLa cells correlated with the increase of MβCD, which is consistent with an increase in PACSIN2-meditated tubule formation upon the increase of MβCD (Fig. 4A,B). Furthermore, we confirmed the decrease of cellular cholesterol upon increasing MβCD treatment by measuring the amount of cholesterol in the cells (Fig. 4C). These results strongly suggested that the regulation of the amount of caveolin-1 was dependent on cholesterol and PACSIN2.

The localization of caveolin-1 in both HeLa cells and the PACSIN2-knockout cells was then examined by immuno-staining using an antibody against caveolin-1. The localization of caveolin-1 in PACSIN2-knockout cells was similar to that of parental HeLa cells under the confocal microscope. After 3 h of MβCD treatment, the cellular localization of caveolin-1 was examined. More cells showed internalized caveolin-1 from the plasma membrane in HeLa cells upon increasing MβCD treatment (Fig. 4D,E). Importantly, caveolin-1 remained on the plasma membrane in the PACSIN2-

Journal of Cell Science (2020) 133, jcs246785. doi:10.1242/jcs.246785

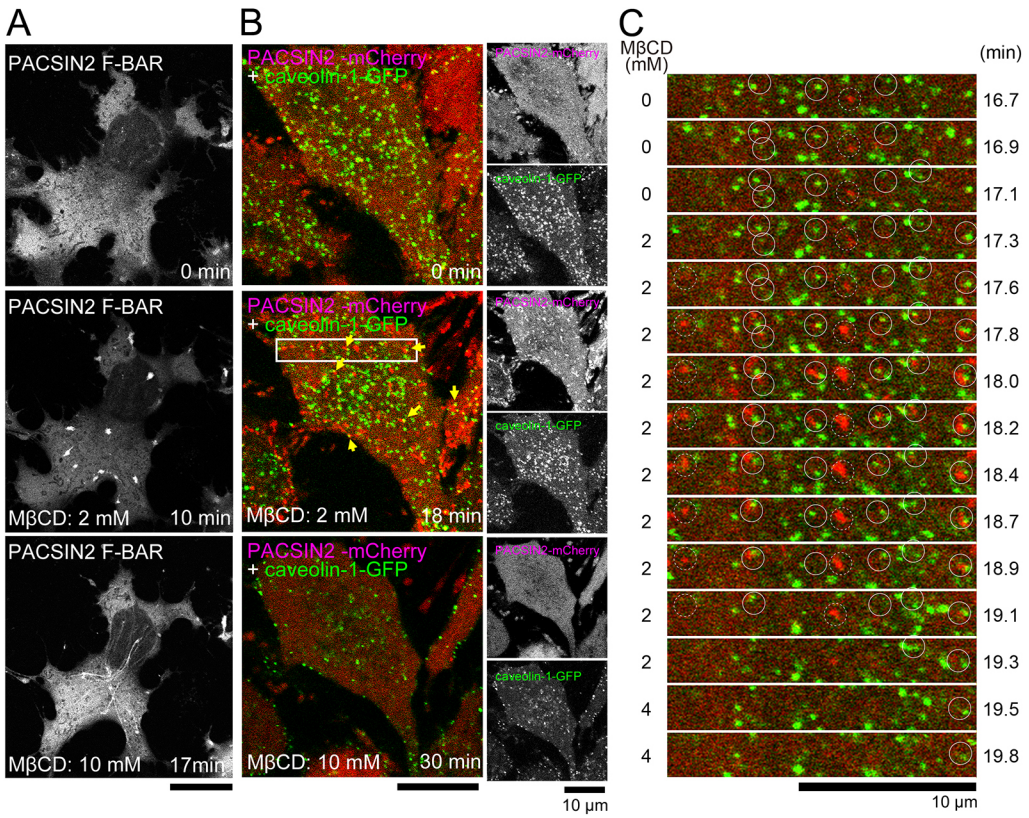

Fig. 3. Formation of PACSIN2 tubules upon cholesterol depletion. (A) HeLa cells expressing the PACSIN2 F-BAR domain fragment showing acute tubulations after treatment with methyl-β-cyclodextrin (MβCD). The tubulation was observed to appear after the cells were treated with MβCD. MβCD was increased in a stepwise manner of 2 mM per 130 s to 10 mM. (B) HeLa cells expressing PACSIN2–mCherry and caveolin-1–GFP after (MβCD) treatment show acute tubulation with caveolin-1 present at the tip of the tubules. PACSIN2 was transiently recruited to the caveolin-1-associated membrane (denoted by yellow arrows) and impaired the morphology of caveolae. This was followed by a decrease in the number of caveolae. MβCD was increased in a stepwise manner of 2 mM per 130 s to 10 mM. The rectangle indicates the region shown in C. (C) The time course and the enlargement of the rectangle in B. The white circles indicate areas with caveolin-1 that had PACSIN2 tubules. The white dashed circles indicate the PACSIN2-associated tubules without detectable levels of caveolin-1. Scale bars: 10 μm.

knockout cells after MβCD treatment (Fig. 4D,E), suggesting that PACSIN2 mediates the internalization of the caveolin-1 from the plasma membrane upon cholesterol depletion. These results suggest that PACSIN2 mediates the internalization of caveolin-1 in the plasma membrane upon the depletion of cholesterol.

DISCUSSION

In this study, we found that the membrane binding of PACSIN2 was weaker when the membrane contained cholesterol, using the reconstituted membrane containing lipids that are abundant in caveolae such as palmitoyl-oleoyl (PO) PC, POPS and cholesterol. This observation suggests that cholesterol depletion strengthens the membrane binding of PACSIN2, thereby inducing tubule formation of caveolae and resulting in the internalization of caveolae, presumably through their endocytosis, i.e. the scission of the tubules.

The localization of PACSIN2 at the neck of caveolar invaginations, but not at the entire caveolar flask (Senju et al., 2011), appears to be consistent with the negative regulation of membrane binding by cholesterol. Although the concentration of cholesterol at the neck of caveolae is unknown, the neck region as the boundary of caveolae is thought to have smaller amounts of cholesterol than the caveolar bulb, because caveolae have a higher concentration of cholesterol than plasma membrane (Ortegren et al., 2004; Razani et al., 2002; Smart et al., 1999). Interestingly, our electron microscopy observations of liposomes with or without cholesterol in the presence of PACSIN2 imply that cholesterol can modulate the membrane-shaping ability of PACSIN2. The POPC/POPS/cholesterol liposomes were deformed by the PACSIN2 F-BAR domain into a ‘beads on a string’ morphology. This beads on a string morphology was previously reported in bovine brain Folch liposomes, which contain cholesterol (Wang et al., 2009). In contrast, the POPC/POPS liposomes without cholesterol were deformed by the PACSIN2 F-BAR domain into straight tubules, which was indicative of tubule formation, as seen in cells. It is possible that the cholesterol in the membrane changes the deformability of the membrane, as indicated by the differences in the packing defect (Fig. 1A) and the rigidity (Dimova, 2014).

The differences in binding appeared to be correlated to the presence of cholesterol in the membrane. Molecular dynamics simulations suggested that the presence of cholesterol can increase the number of packing defects in the membrane, while tightening the packing of the entire membrane, which is suggested to occur because of the tight packing of phospholipids through the association of cholesterol with the acyl-chain of phospholipids (Falck et al., 2004; Lund-Katz et al., 1988; Presti et al., 1982). The hydrophobic loops of PACSIN2 F-BAR domain are thought to insert into the packing defects in the membrane (Shimada et al., 2010). Therefore, an increase in packing defects was first hypothesized to lead to an increase in the binding of PACSIN2 to the cell membrane. It was possible that an increase of packing defects would occur upon the

Journal of Cell Science (2020) 133, jcs246785. doi:10.1242/jcs.246785

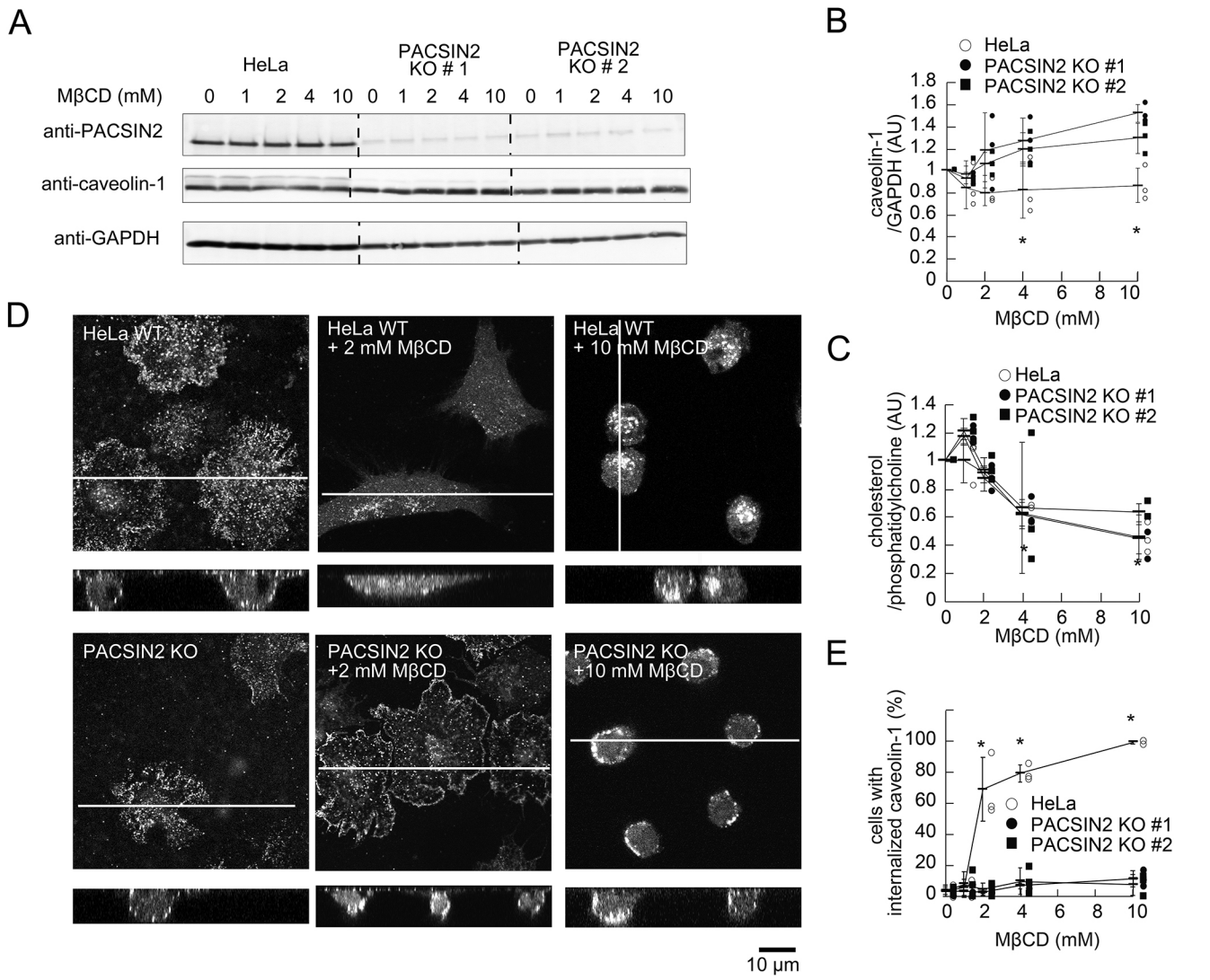

Fig. 4. Internalization of caveolin-1 upon depletion of cholesterol is mediated by PACSIN2. (A) HeLa cells and the two lines of PACSIN2-knockout cells were treated with 10 mM MβCD for 3 h. The amounts of PACSIN2, caveolin-1, and GAPDH were analyzed by western blotting. (B) Quantification of A, showing alterations of the amount of caveolin-1 upon MβCD treatment. The amount of caveolin-1 relative to GAPDH was examined and the fold changes by MβCD are shown. *n*=3. Error bar indicates the s.d. **P*<0.05 (one-way ANOVA followed by Tukey's post hoc test) between the HeLa cells and the PACSIN2-knockout cells at each MβCD concentration. (C) The amount of cholesterol relative to phosphatidylcholine. The amounts of cholesterol and phosphatidylcholine were measured after lysis of the cells. *n*=3. Error bar indicates the s.d. **P*<0.05 (one-way ANOVA followed by Tukey's post hoc test) compared to the cells without MβCD treatment (0 mM). (D) Caveolin-1 distribution in HeLa cells and PACSIN2-knockout cells after treatment with MβCD (10 mM). The cells were fixed and labeled with anti-caveolin-1 antibody. The white line indicates the sectioning plane in the lower panels. (E) Quantification of D, showing the percentage of cells with stronger caveolin-1 staining in cytoplasm than on the plasma membrane. *n*=3. Error bar indicates the s.d. **P*<0.05 (one-way ANOVA followed by Tukey's post hoc test) compared to the HeLa cells without MβCD treatment (0 mM).

application of tension to the membrane. However, the results of molecular dynamics simulation and leakage assay indicated that the tension before membrane rupture did not increase the packing defects nor the rate of PACSIN2 binding to the membrane. Although the mutation at the loop results in reduced binding of PACSIN2 to the membrane (Shimada et al., 2010), our results suggest that the charge density, and not the packing defects, could be the primary determinant of PACSIN2 membrane binding.

It is widely known that caveolae are cholesterol-dependent structures (Fielding and Fielding, 2000; Harder and Simons, 1997; Hooper, 1999). However, the mechanisms of the cholesterol-dependent regulation of caveolae have not yet been elucidated. In this study, the formation of tubules as a result of cholesterol depletion suggested a mechanism of caveolar downregulation upon cholesterol depletion. It should be noted that not all of caveolae were positive for PACSIN2 (Hansen et al., 2011; Seemann et al., 2017; Senju et al., 2011), which might imply that only caveolae with relatively small amounts of cholesterol are regulated by PACSIN2. Tubule formation will recruit more dynamin to the neck of caveolae, which is thought to induce the scission of caveolae, leading to their internalization, because PACSIN2-mediated tubule formation is increased upon the expression of inactive dynamin (Senju et al., 2011). It is also possible that the longer tubules are more susceptible to fission by mechanical forces, which also might induce the scission of caveolae for their internalization, as has been reported for endophilin-mediated tubule formation (Simunovic et al., 2017). Caveolae are thought to be transported to endosomes after internalization, where the degradation takes place (Kiss and

Journal of Cell Science (2020) 133, jcs246785. doi:10.1242/jcs.246785

Botos, 2009; Parton, 2004), which would result in the cholesterol-dependent downregulation of caveolae.

MATERIALS AND METHODS

Molecular dynamics

Initial bilayers containing 400 lipid/cholesterol molecules (200 molecules in each leaflet), and with 22.5-Å-thick layers of water molecules and 150 mM NaCl at the top and bottom of the bilayers, were constructed using a CHARMM-GUI membrane builder (Wu et al., 2014). The lipid/cholesterol compositions of the simulated systems are shown in Fig. 1A. We also constructed a two-bilayer systems (with tension in Fig. 1A) to investigate the effects of tension induced by the osmotic pressure. After 500-ns molecular dynamics (MD) simulations, the single-bilayer systems were replicated along the bilayer normal direction. Then, randomly selected water molecules were replaced with Na^+ or Cl^- so that the two regions divided by the two bilayers had different concentrations of NaCl (150 and 230 mM). All MD simulations were performed using Gromacs 2018.1 (Abraham et al., 2015; Berendsen et al., 1995). The system was brought to thermodynamic equilibrium at 300 K and 1 atm using the Nosé–Hoover thermostat and the Parrinello–Rahman barostat with semi-isotropic pressure control. The equations of motion were integrated with a time step of 2 fs. Long-range Coulomb energy was evaluated using the particle mesh Ewald (PME) method. The CHARMM36m force field (Huang et al., 2017) was used. Simulations were conducted for 500 ns, and trajectories were saved every 0.1 ns.

To detect the packing defects, we followed the procedure by Vamparys et al. (2013). We used 4 Å for vdW radii of carbon and phosphorus atoms and 3 Å for those of oxygen and nitrogen atoms. The last 300-ns (3000 snapshots) were used for the analysis. To evaluate a fraction of the defect area, we defined a fraction as the sum of the defect area equal to or larger than 10 $Å^2$.

GST-tagged protein purification

E. coli Rosetta Gami B-containing the pGEX6P1-PACSIN2 (aa 1–343) construct (Shimada et al., 2010) were cultured in LB medium overnight at 20°C after the addition of IPTG. GST-tagged expressed proteins were purified using GST beads (glutathione–Sepharose 4B; GE Healthcare Life Science). On the following day, the cells were centrifuged, and the resulting pellets were stored at −80°C as the stocks. Before purification, GST beads were washed with *E. coli* sonication buffer (10 mM Tris-HCl pH 7.5, 150 mM NaCl, 1 mM EDTA, 0.5% Triton X-100, Milli Q water) three times (Hanawa-Suetsugu et al., 2019). To purify the proteins, the cell pellets were resuspended in a mixture of the sonication buffer, 0.1 mM DTT and 1 mM PMSF, followed by sonication in an ice container to disrupt the cell membrane (3-s burst–3-s rest for total time 4 min). The lysates were then centrifuged at 20,400 ***g*** for 10 min at 4°C. The supernatant was transferred into a suspension of GST beads and rotated for 1 h at 4°C. The beads were then centrifuged at 500 ***g*** for 5 min at 4°C, the supernatant was discarded, and the beads were suspended in the wash buffer (10 mM Tris HCl pH 7.5, 150 mM NaCl, 1 mM EDTA). The washing of the beads was repeated over three times. Subsequently, PreScission Protease (GE Healthcare) was added to remove GST from the proteins, followed by overnight rotation at 4°C. The protein was then separated from the GST beads using a mini column before storage as a stock solution at −80°C. The purified proteins were visualized using an SDS-PAGE gel and Coomassie Brilliant Blue (CBB) staining. The protein concentration was determined using the band intensities of the gels in Image J.

Liposome preparation

Liposomes were prepared from 1-palmitoyl-2-oleoyl-sn-glycero-3-phosphocholine (POPC), 1-palmitoyl-2-oleoyl-sn-glycero-3-phospho-L-serine (POPS), and cholesterol. POPC (850457, Avanti polar lipids), POPS (840034, Avanti polar lipids) and cholesterol (C8667, Sigma) were purchased. These lipids were mixed at the ratios of 60:40:0, 54:36:10, 42:28:30, and 33:22:45 to obtain the liposomes of POPC/POPS, POPC/POPS/Chol(10), POPC/POPS/Chol(30), and POPC/POPS/Chol(45). To obtain the liposomes, the lipids were dried under nitrogen gas, followed by drying in a vacuum for at least 1 h to remove any traces of residual solvent. Then, 300 or 460 mOsmol/kg sucrose buffer (300 or 460 mM sucrose, 10 mM Tris-HCl pH 7.5 and 1 mM EDTA) was added to the thin layer of dried lipids, followed by vortexing to induce liposome formation. The liposome suspension was subjected to ten freeze–thaw cycles in liquid nitrogen, followed by thawing in a water bath at 45°C and either storage at −30°C or immediate use in the assays. Before use, the liposomes were extruded through a polycarbonate membrane with a pore size of 2 µm.

Liposome co-sedimentation assay

The liposomes used in this assay were composed of POPC/POPS and POPC/POPS/cholesterol. Proteins were mixed with the liposomes. The osmolarity was adjusted using a buffer with various concentrations of glucose (0–160 mM glucose, 10 mM Tris-HCl pH 7.5, 1 mM EDTA, 150 mM NaCl) to obtain isotonic (300 mOsmol/kg inside and outside liposome) and hypotonic conditions (460 mOsmol/kg inside and 300 mOsmol/kg outside liposome). The mixture was then incubated with protein at room temperature for 20 min, followed by centrifugation at 50,000 rpm for 20 min at 25°C in a TLA100 rotor (Beckman Coulter). Following these procedures, any bound proteins would be found in the pellet, while unbound proteins would be found in the supernatant. The pellet and supernatant were then separated, subjected to SDS-PAGE and stained using CBB.

Lamellarity of liposome membrane by NBD-lipid quenching assay

The lamellarity of liposome membrane was estimated by an NBD-lipid quenching assay (McIntyre and Sleight, 1991). Liposomes were prepared by including 1,2-dioleoyl-sn-glycero-3-phosphoethanolamine-N-(7-nitro-2-1,3-benzoxadiazol-4-yl) (NBD-DOPE, Avanti polar lipid) as 1% of total lipids. After freeze-thawing, the NBD intensity of liposomes (0.1 ml of 0.01 mg/ml total lipids) was measured with a fluorescence spectrometer (FP-6500, JASCO, Japan, ex=465 nm, em=535 nm). Then, a 1/20 volume of 1 M dithionite (sodium hydrosulfite, Nacalai, Japan) was added to quench the NBD-DOPE on the outer leaflet. Next, a 1/50 volume of 20% Triton X-100 was added to solubilize the liposomes, resulting in the quenching of the NBD-DOPE of the inner leaflet. The fluorescent intensity was normalized between the mean intensities before quenching and after the addition of Triton X-100.

Transmission electron microscopy

Proteins and liposomes were prepared and mixed as in the liposome co-sedimentation assay, then placed on a parafilm surface on a heating block at 25°C. After incubation for 20 min, the samples were placed on a grid (Nisshin EM) covered with polyvinyl formal (Formvar; Nisshin EM). NaCl was then removed using HEPES buffer, and the samples were stained with 0.5% uranyl acetate before air-drying for several hours to remove the remaining solutions. Dried sections were then observed using a transmission electron microscope (Hitachi H-7100).

Osmotically induced leakage assay

The lipids used in these experiments were porcine brain Folch, 1-palmitoyl-2-oleoyl-sn-glycero-3-phosphocholine (POPC), 1-palmitoyl-2-oleoyl-sn-glycero-3-phospho-L-serine (POPS), and cholesterol dissolved in chloroform (Avanti Polar Lipids). These lipids were dried under nitrogen gas, followed by drying in vacuum for 20 min. The dried lipids were suspended in 300 µl of the buffer containing the indicated concentrations of NaCl, 10 mM Tris-HCl pH 7.5, 1 mM EDTA and 20 µM 5(6)-carboxyfluorescein (CF) for 1–2 h. The osmolarity inside and outside the liposomes was adjusted using the concentration of NaCl. The Sephadex G-50 suspension was then settled in a chromatography column. The liposomes were added to the column, and the CF outside the liposomes was removed. The eluate drops were collected in Eppendorf tubes for the elution of the CF phase. The tubes containing liposomes loaded with CF were verified under a UV light. These liposomes were then collected in a single Eppendorf tube and divided into three treatment groups: isotonic conditions, hypotonic conditions and liposomes, for the determination of total CF. All of the groups were centrifuged at 109,000 ***g*** for 20 min, and the resulting

supernatant was removed. The pellet of the first group was resuspended with isotonic NaCl or glucose buffer, while the pellet of the second group was resuspended with hypotonic buffer. Both groups were incubated at room temperature for 20 min, followed by centrifugation at 109,000 ***g*** for 20 min. The fluorescence intensity of the supernatant was measured using a spectrofluorometer (Jasco FP-6500). The third group was resuspended using the buffer with detergent (10 mM Tris-HCl pH 7.5, 150 mM NaCl, 1 mM EDTA and 0.5% Triton X-100) for at least 10 min to allow for the release of CF from the liposomes. The fluorescence intensity of CF was measured as the percentage of the total CF. Total CF leakage from liposome was calculated using the following formula:

$$\text{Leakage}(\%) = 100 \times \frac{F_{\text{hypo}} - F_{\text{iso}}}{F_{\text{total}} - F_{\text{iso}}},$$

where F_{hypo}, F_{iso}, and F_{total} denote the CF intensity of hypotonic, isotonic, and total CF in liposomes, respectively. The buffer osmolality was confirmed using a Wescor Vapro 5600 vapor pressure osmometer, according to manufacturer's protocol. The unit of measurement was mOsmol/kg.

Cell culture and MβCD treatment

HeLa cells (Senju et al., 2015), from ATCC, were cultured in Dulbecco's modified Eagle's medium (DMEM) (Nacalai) supplemented with 10% fetal calf serum (FCS), penicillin and streptomycin (Meiji pharmaceuticals). For MβCD treatment, the HeLa cells were suspended in DMEM supplemented with 1/100 concentration of insulin, transferrin and selenium solution (ITS-G) (Gibco 41400045) and cultured overnight. MβCD (Sigma) was then added to the cells at 1, 2, 4 and 10 mM for 3 h. The cells were stained or were analyzed by western blotting by using anti-PACSIN2 antibody (Senju et al., 2011), anti-caveolin-1 antibody (Cell Signaling, D46G3, #3267), and anti-GAPDH antibody (Santa Cruz Biotechnology, H-12,sc-16657).

Expression of PACSIN2 in HeLa cells

EGFP-labeled PACSIN2 in pEGFP-C1 (Senju et al., 2015) was transfected using Lipofectamine 3000 and PLUS reagents (Invitrogen), according to the manufacturer's instructions. mCherry-labeled PACSIN2 was prepared by subcloning PACSIN2 cDNA into pmCherry-C1 vector (Clontech), in which the GFP in pEGFP-C1 was replaced with mCherry. Cells stably expressing caveolin-1–EGFP were prepared as previously described (Senju et al., 2015). The stable expression of PACSIN2–mCherry in the caveolin-1–EGFP-expressing HeLa cells (Morén et al., 2012) was performed using the pMXs vector and retrovirus that was produced in the packaging cell line Plat-A (Kitamura et al., 2003). After the FACS sorting and cloning of the cells, the cells with PACSIN2–mCherry expression similar to the endogenous PACSIN2 level were selected for observation using western blotting.

Live observation

For live observation using total internal reflection microscopy, HeLa cells were grown on a glass-bottomed dish using DMEM containing 10% FBS and 10 mM HEPES (pH 7.5). Images were acquired for 5 min at 1 or 0.5 s intervals using a confocal microscope (Olympus FV1000D) equipped with a 100× NA 1.45 oil immersion objective (Olympus). Live cells were treated with 10 mM methyl-β-cyclodextrin (MβCD), which were added in 5 times with 2 mM/130 s.

PACSIN2-knockout cells

The guide RNA targeting the first exon of PACSIN2 (TGAGCGGGCGC-GCATCGAGA) was designed using the MIT CRISPR server (http://crispr.mit.edu) (Hsu et al., 2013) and inserted into the pX459 vector (Ran et al., 2013). After transfection into HeLa cells, the cells were cloned by puromycin resistance.

Immunofluorescence staining

Cells grown on poly-L-lysine-coated cover glasses were fixed with 4% paraformaldehyde with 0.2% glutaraldehyde in HEPES-buffered saline, containing 30 mM HEPES (pH 7.5), 100 mM NaCl, and 2 mM $CaCl_2$ for 5 min. The cells were then blocked with DMEM supplemented with 10% fetal calf serum (FCS) overnight and incubated with anti-caveolin-1 antibody (BD, BD610406) in 1% BSA in TBS (100 mM Tris-HCl pH 7.5 and 150 mM NaCl) for 1 h. After washing with PBS, the cells were incubated with fluorescently labeled secondary antibody. The cells were washed again before mounting using Prolong Gold (Thermo Fisher/Invitrogen). Cell images were obtained using an FV1000 laser-scanning confocal microscope (Olympus) equipped with a 100× NA 1.45 oil lens (Olympus) at room temperature.

Measurement of cholesterol of the cells

Cells were harvested in buffer containing 10 mM Tris-HCl pH 7.5, 500 mM NaCl and 10% Triton X-100, and then the amounts of cholesterol and phosphatidylcholine were measured with LabAssay™ Cholesterol (FUJIFILM Wako, 294-65801) and LabAssay™ Phospholipids (FUJIFILM Wako, 294-63801), respectively. The amount of cholesterol was expressed as a relative amount to that of phosphatidylcholine.

Statistical analysis

Experiments were performed at least in triplicate. The results were presented as the mean±standard deviation (s.d.). Statistical significance was analyzed using a one-way ANOVA followed by Tukey's post hoc test (Figs 1F, 4B,C, E and Fig. S2D) or two-tailed Student's *t*-test (Fig. 1G). The half maximum of the binding was determined using Excel solver. $P<0.05$ was considered statistically significant.

Acknowledgements

We thank all our lab members for helpful discussion and continuous support of this work.

Competing interests

The authors declare no competing or financial interests.

Author contributions

Conceptualization: S.S.; Methodology: K.T., T.I., A.K.; Software: K.T., A.K.; Validation: S.Y.L., T.I., A.K., S.S.; Formal analysis: A.G., S.Y.L.; Investigation: A.G., K.T., S.Y.L., T.I., K.H.-S., K.O.-Y., K.Y., S.S.; Resources: K.T., K.Y.; Data curation: A.G., K.T., A.K., S.S.; Writing - original draft: A.G., S.Y.L., T.I., S.S.; Writing - review & editing: S.Y.L., K.Y., A.K., S.S.; Visualization: A.G., S.Y.L., T.I.; Supervision: K.Y., A.K., S.S.; Project administration: A.K., S.S.; Funding acquisition: A.K., S.S.

Funding

This work was supported by grants from the Funding Program for Next Generation World-Leading Researchers (NEXT program LS031), Japan Society for the Promotion of Science (JSPS) (KAKENHI 26291037, JP15H0164, JP15H05902, JP17H03674, JP17H06006), Japan Science and Technology Agency (JST CREST) (JPMJCR1863), and the Nara Institute of Science and Technology (NAIST) Interdisciplinary Frontier Research Project to S.S. This research was supported by JSPS KAKENHI (JP19H03191) and Ministry of Education, Culture, Sports, Science and Technology (MEXT) Priority Issues on Post-K Computer Projects 'Building Innovative Drug Discovery Infrastructure through Functional Control of Biomolecular System' to A.K. The computations were partly performed using the supercomputers at the RCCS at the National Institute of Natural Science and ISSP at the University of Tokyo. This research also used computational resources of the K computer provided by the RIKEN Advanced Institute for Computational Science through the HPCI System Research project (Project ID: hp190181).

Supplementary information

Supplementary information available online at https://jcs.biologists.org/lookup/doi/10.1242/jcs.246785.supplemental

Peer review history

The peer review history is available online at https://jcs.biologists.org/lookup/doi/10.1242/jcs.246785.reviewer-comments.pdf

References

Abraham, M. J., Murtola, T., Schulz, R., Páll, S., Smith, J. C., Hess, B. and Lindahl, E. (2015). GROMACS: high performance molecular simulations through multi-level parallelism from laptops to supercomputers. *SoftwareX* **1-2**, 19-25. doi:10.1016/j.softx.2015.06.001

Alam Shibly, S. U., Ghatak, C., Sayem Karal, M. A., Moniruzzaman, M. and Yamazaki, M. (2016). Experimental estimation of membrane tension induced by osmotic pressure. *Biophys. J.* **111**, 2190-2201. doi:10.1016/j.bpj.2016.09.043

Berendsen, H. J. C., van der Spoel, D. and van Drunen, R. (1995). GROMACS: a message-passing parallel molecular dynamics implementation. *Comput. Phys. Commun.* **91**, 43-56. doi:10.1016/0010-4655(95)00042-E

Breen, M. R., Camps, M., Carvalho-Simoes, F., Zorzano, A. and Pilch, P. F. (2012). Cholesterol depletion in adipocytes causes caveolae collapse concomitant with proteosomal degradation of cavin-2 in a switch-like fashion. *PLoS ONE* **7**, e34516. doi:10.1371/journal.pone.0034516

Cai, Q., Guo, L., Gao, H. and Li, X.-A. (2013). Caveolar fatty acids and acylation of caveolin-1. *PLoS ONE* **8**, e60884. doi:10.1371/journal.pone.0060884

Daumke, O., Roux, A. and Haucke, V. (2014). BAR domain scaffolds in dynamin-mediated membrane fission. *Cell* **156**, 882-892. doi:10.1016/j.cell.2014.02.017

Dharmalingam, E., Haeckel, A., Pinyol, R., Schwintzer, L., Koch, D., Kessels, M. M. and Qualmann, B. (2009). F-BAR proteins of the syndapin family shape the plasma membrane and are crucial for neuromorphogenesis. *J. Neurosci.* **29**, 13315-13327. doi:10.1523/JNEUROSCI.3973-09.2009

Dimova, R. (2014). Recent developments in the field of bending rigidity measurements on membranes. *Adv. Colloid Interface Sci.* **208**, 225-234. doi:10.1016/j.cis.2014.03.003

Doherty, G. J. and McMahon, H. T. (2009). Mechanisms of endocytosis. *Annu. Rev. Biochem.* **78**, 857-902. doi:10.1146/annurev.biochem.78.081307.110540

Dreja, K., Voldstedlund, M., Vinten, J., Tranum-Jensen, J., Hellstrand, P. and Swärd, K. (2002). Cholesterol depletion disrupts caveolae and differentially impairs agonist-induced arterial contraction. *Arterioscler. Thromb. Vasc. Biol.* **22**, 1267-1272. doi:10.1161/01.ATV.0000023438.32585.A1

Fairn, G. D., Schieber, N. L., Ariotti, N., Murphy, S., Kuerschner, L., Webb, R. I., Grinstein, S. and Parton, R. G. (2011). High-resolution mapping reveals topologically distinct cellular pools of phosphatidylserine. *J. Cell Biol.* **194**, 257-275. doi:10.1083/jcb.201012028

Falck, E., Patra, M., Karttunen, M., Hyvönen, M. T. and Vattulainen, I. (2004). Lessons of slicing membranes: interplay of packing, free area, and lateral diffusion in phospholipid/cholesterol bilayers. *Biophys. J.* **87**, 1076-1091. doi:10.1529/biophysj.104.041368

Fielding, C. J. and Fielding, P. E. (2000). Cholesterol and caveolae: structural and functional relationships. *Biochim. Biophys. Acta* **1529**, 210-222. doi:10.1016/S1388-1981(00)00150-5

Finkelstein, A., Zimmerberg, J. and Cohen, F. S. (1986). Osmotic swelling of vesicles: its role in the fusion of vesicles with planar phospholipid bilayer membranes and its possible role in exocytosis. *Annu. Rev. Physiol.* **48**, 163-174. doi:10.1146/annurev.ph.48.030186.001115

Hailstones, D., Sleer, L. S., Parton, R. G. and Stanley, K. K. (1998). Regulation of caveolin and caveolae by cholesterol in MDCK cells. *J. Lipid Res.* **39**, 369-379.

Hamai, C., Cremer, P. S. and Musser, S. M. (2007). Single giant vesicle rupture events reveal multiple mechanisms of glass-supported bilayer formation. *Biophys. J.* **92**, 1988-1999. doi:10.1529/biophysj.106.093831

Hanawa-Suetsugu, K., Itoh, Y., Ab Fatah, M., Nishimura, T., Takemura, K., Takeshita, K., Kubota, S., Miyazaki, N., Wan Mohamad Noor, W. N. I., Inaba, T. et al. (2019). Phagocytosis is mediated by two-dimensional assemblies of the F-BAR protein GAS7. *Nat. Commun.* **10**, 4763. doi:10.1038/s41467-019-12738-w

Hansen, C. G., Howard, G. and Nichols, B. J. (2011). Pacsin 2 is recruited to caveolae and functions in caveolar biogenesis. *J. Cell Sci.* **124**, 2777-2785. doi:10.1242/jcs.084319

Harder, T. and Simons, K. (1997). Caveolae, DIGs, and the dynamics of sphingolipid-cholesterol microdomains. *Curr. Opin. Cell Biol.* **9**, 534-542. doi:10.1016/S0955-0674(97)80030-0

Henriksen, J., Rowat, A. C. and Ipsen, J. H. (2004). Vesicle fluctuation analysis of the effects of sterols on membrane bending rigidity. *Eur. Biophys. J.* **33**, 732-741. doi:10.1007/s00249-004-0420-5

Henriksen, J., Rowat, A. C., Brief, E., Hsueh, Y. W., Thewalt, J. L., Zuckermann, M. J. and Ipsen, J. H. (2006). Universal behavior of membranes with sterols. *Biophys. J.* **90**, 1639-1649. doi:10.1529/biophysj.105.067652

Hill, M. M., Bastiani, M., Luetterforst, R., Kirkham, M., Kirkham, A., Nixon, S. J., Walser, P., Abankwa, D., Oorschot, V. M. J., Martin, S. et al. (2008). PTRF-Cavin, a conserved cytoplasmic protein required for caveola formation and function. *Cell* **132**, 113-124. doi:10.1016/j.cell.2007.11.042

Hirama, T., Das, R., Yang, Y., Ferguson, C., Won, A., Yip, C. M., Kay, J. G., Grinstein, S., Parton, R. G. and Fairn, G. D. (2017). Phosphatidylserine dictates the assembly and dynamics of caveolae in the plasma membrane. *J. Biol. Chem.* **292**, 14292-14307. doi:10.1074/jbc.M117.791400

Hooper, N. M. (1999). Detergent-insoluble glycosphingolipid/cholesterol-rich membrane domains, lipid rafts and caveolae (review). *Mol. Membr. Biol.* **16**, 145-156. doi:10.1080/096876899294607

Hsu, P. D., Scott, D. A., Weinstein, J. A., Ran, F. A., Konermann, S., Agarwala, V., Li, Y., Fine, E. J., Wu, X., Shalem, O. et al. (2013). DNA targeting specificity of RNA-guided Cas9 nucleases. *Nat. Biotechnol.* **31**, 827-832. doi:10.1038/nbt.2647

Huang, J., Rauscher, S., Nawrocki, G., Ran, T., Feig, M., de Groot, B. L., Grubmüller, H. and MacKerell, A. D. Jr. (2017). CHARMM36m: an improved force field for folded and intrinsically disordered proteins. *Nat. Methods* **14**, 71-73. doi:10.1038/nmeth.4067

Hubert, M., Larsson, E. and Lundmark, R. (2020). Keeping in touch with the membrane; protein- and lipid-mediated confinement of caveolae to the cell surface. *Biochem. Soc. Trans.* **48**, 155-163. doi:10.1042/bst20190386

Huot, P. S. P., Sarkar, B. and Ma, D. W. L. (2010). Conjugated linoleic acid alters caveolae phospholipid fatty acid composition and decreases caveolin-1 expression in MCF-7 breast cancer cells. *Nutr. Res.* **30**, 179-185. doi:10.1016/j.nutres.2010.02.003

Khater, I. M., Liu, Q., Chou, K. C., Hamarneh, G. and Nabi, I. R. (2019). Super-resolution modularity analysis shows polyhedral caveolin-1 oligomers combine to form scaffolds and caveolae. *Sci. Rep.* **9**, 9888. doi:10.1038/s41598-019-46174-z

Kiss, A. L. and Botos, E. (2009). Endocytosis via caveolae: alternative pathway with distinct cellular compartments to avoid lysosomal degradation? *J. Cell. Mol. Med.* **13**, 1228-1237. doi:10.1111/j.1582-4934.2009.00754.x

Kitamura, T., Koshino, Y., Shibata, F., Oki, T., Nakajima, H., Nosaka, T. and Kumagai, H. (2003). Retrovirus-mediated gene transfer and expression cloning: powerful tools in functional genomics. *Exp. Hematol.* **31**, 1007-1014. doi:10.1016/S0301-472X(03)00260-1

Koch, D., Westermann, M., Kessels, M. M. and Qualmann, B. (2012). Ultrastructural freeze-fracture immunolabeling identifies plasma membrane-localized syndapin II as a crucial factor in shaping caveolae. *Histochem. Cell Biol.* **138**, 215-230. doi:10.1007/s00418-012-0945-0

Lund-Katz, S., Laboda, H. M., McLean, L. R. and Phillips, M. C. (1988). Influence of molecular packing and phospholipid type on rates of cholesterol exchange. *Biochemistry* **27**, 3416-3423. doi:10.1021/bi00409a044

McIntyre, J. C. and Sleight, R. G. (1991). Fluorescence assay for phospholipid membrane asymmetry. *Biochemistry* **30**, 11819-11827. doi:10.1021/bi00115a012

Morén, B., Shah, C., Howes, M. T., Schieber, N. L., McMahon, H. T., Parton, R. G., Daumke, O. and Lundmark, R. (2012). EHD2 regulates caveolar dynamics via ATP-driven targeting and oligomerization. *Mol. Biol. Cell* **23**, 1316-1329. doi:10.1091/mbc.e11-09-0787

Murata, M., Peranen, J., Schreiner, R., Wieland, F., Kurzchalia, T. V. and Simons, K. (1995). VIP21/caveolin is a cholesterol-binding protein. *Proc. Natl. Acad. Sci. USA* **92**, 10339-10343. doi:10.1073/pnas.92.22.10339

Nishimura, T., Morone, N. and Suetsugu, S. (2018). Membrane re-modelling by BAR domain superfamily proteins via molecular and non-molecular factors. *Biochem. Soc. Trans.* **46**, 379-389. doi:10.1042/BST20170322

Ohtani, Y., Irie, T., Uekama, K., Fukunaga, K. and Pitha, J. (1989). Differential effects of alpha-, beta- and gamma-cyclodextrins on human erythrocytes. *Eur. J. Biochem.* **186**, 17-22. doi:10.1111/j.1432-1033.1989.tb15171.x

Ortegren, U., Karlsson, M., Blazic, N., Blomqvist, M., Nystrom, F. H., Gustavsson, J., Fredman, P. and Stralfors, P. (2004). Lipids and glycosphingolipids in caveolae and surrounding plasma membrane of primary rat adipocytes. *Eur. J. Biochem.* **271**, 2028-2036. doi:10.1111/j.1432-1033.2004.04117.x

Parpal, S., Karlsson, M., Thorn, H. and Strålfors, P. (2001). Cholesterol depletion disrupts caveolae and insulin receptor signaling for metabolic control via insulin receptor substrate-1, but not for mitogen-activated protein kinase control. *J. Biol. Chem.* **276**, 9670-9678. doi:10.1074/jbc.M007454200

Parton, R. G. (2004). Caveolae meet endosomes: a stable relationship? *Dev. Cell* **7**, 458-460. doi:10.1016/j.devcel.2004.09.009

Patel, H. H. and Insel, P. A. (2009). Lipid rafts and caveolae and their role in compartmentation of redox signaling. *Antioxid. Redox Signal.* **11**, 1357-1372. doi:10.1089/ars.2008.2365

Pelkmans, L. and Zerial, M. (2005). Kinase-regulated quantal assemblies and kiss-and-run recycling of caveolae. *Nature* **436**, 128-133. doi:10.1038/nature03866

Pike, L. J. (2003). Lipid rafts: bringing order to chaos. *J. Lipid Res.* **44**, 655-667. doi:10.1194/jlr.R200021-JLR200

Pike, L. J., Han, X. and Gross, R. W. (2005). Epidermal growth factor receptors are localized to lipid rafts that contain a balance of inner and outer leaflet lipids: a shotgun lipidomics study. *J. Biol. Chem.* **280**, 26796-26804. doi:10.1074/jbc.M503805200

Presti, F. T., Pace, R. J. and Chan, S. I. (1982). Cholesterol-phospholipid interaction in membranes. 2. Stoichiometry and molecular packing of cholesterol-rich domains. *Biochemistry* **21**, 3831-3835. doi:10.1021/bi00259a017

Puri, V., Watanabe, R., Singh, R. D., Dominguez, M., Brown, J. C., Wheatley, C. L., Marks, D. L. and Pagano, R. E. (2001). Clathrin-dependent and -independent internalization of plasma membrane sphingolipids initiates two Golgi targeting pathways. *J. Cell Biol.* **154**, 535-547. doi:10.1083/jcb.200102084

Ran, F. A., Hsu, P. D., Wright, J., Agarwala, V., Scott, D. A. and Zhang, F. (2013). Genome engineering using the CRISPR-Cas9 system. *Nat. Protoc.* **8**, 2281-2308. doi:10.1038/nprot.2013.143

Rao, Y., Ma, Q., Vahedi-Faridi, A., Sundborger, A., Pechstein, A., Puchkov, D., Luo, L., Shupliakov, O., Saenger, W. and Haucke, V. (2010). Molecular basis for SH3 domain regulation of F-BAR-mediated membrane deformation. *Proc. Natl. Acad. Sci. USA* **107**, 8213-8218. doi:10.1073/pnas.1003478107

Razani, B., Woodman, S. E. and Lisanti, M. P. (2002). Caveolae: from cell biology to animal physiology. *Pharmacol. Rev.* **54**, 431-467. doi:10.1124/pr.54.3.431

Rothberg, K. G., Heuser, J. E., Donzell, W. C., Ying, Y.-S., Glenney, J. R. and Anderson, R. G. W. (1992). Caveolin, a protein component of caveolae membrane coats. *Cell* **68**, 673-682. doi:10.1016/0092-8674(92)90143-Z

Schlegel, A., Schwab, R. B., Scherer, P. E. and Lisanti, M. P. (1999). A role for the caveolin scaffolding domain in mediating the membrane attachment of caveolin-1. The caveolin scaffolding domain is both necessary and sufficient for membrane binding in vitro. *J. Biol. Chem.* **274**, 22660-22667. doi:10.1074/jbc.274.32.22660

Seemann, E., Sun, M., Krueger, S., Tröger, J., Hou, W., Haag, N., Schüler, S., Westermann, M., Huebner, C. A., Romeike, B. et al. (2017). Deciphering caveolar functions by syndapin III KO-mediated impairment of caveolar invagination. *eLife* **6**, e29854. doi:10.7554/elife.29854

Senju, Y. and Suetsugu, S. (2015). Possible regulation of caveolar endocytosis and flattening by phosphorylation of F-BAR domain protein PACSIN2/syndapin II. *Bioarchitecture* **5**, 70-77. doi:10.1080/19490992.2015.1128604

Senju, Y., Itoh, Y., Takano, K., Hamada, S. and Suetsugu, S. (2011). Essential role of PACSIN2/syndapin-II in caveolae membrane sculpting. *J. Cell Sci.* **124**, 2032-2040. doi:10.1242/jcs.086264

Senju, Y., Rosenbaum, E., Shah, C., Hamada-Nakahara, S., Itoh, Y., Yamamoto, K., Hanawa-Suetsugu, K., Daumke, O. and Suetsugu, S. (2015). Phosphorylation of PACSIN2 by protein kinase C triggers the removal of caveolae from the plasma membrane. *J. Cell Sci.* **128**, 2766-2780. doi:10.1242/jcs.167775

Shimada, A., Takano, K., Shirouzu, M., Hanawa-Suetsugu, K., Terada, T., Toyooka, K., Umehara, T., Yamamoto, M., Yokoyama, S. and Suetsugu, S. (2010). Mapping of the basic amino-acid residues responsible for tubulation and cellular protrusion by the EFC/F-BAR domain of pacsin2/Syndapin II. *FEBS Lett.* **584**, 1111-1118. doi:10.1016/j.febslet.2010.02.058

Shoemaker, S. D. and Vanderlick, T. K. (2002). Stress-induced leakage from phospholipid vesicles: effect of membrane composition. *Ind. Eng. Chem. Res.* **41**, 324-329. doi:10.1021/ie010049t

Simons, K. and Toomre, D. (2000). Lipid rafts and signal transduction. *Nat. Rev. Mol. Cell Biol.* **1**, 31-39. doi:10.1038/35036052

Simunovic, M., Voth, G. A., Callan-Jones, A. and Bassereau, P. (2015). When physics takes over: BAR proteins and membrane curvature. *Trends Cell Biol.* **25**, 780-792. doi:10.1016/j.tcb.2015.09.005

Simunovic, M., Manneville, J.-B., Renard, H.-F., Evergren, E., Raghunathan, K., Bhatia, D., Kenworthy, A. K., Voth, G. A., Prost, J., McMahon, H. T. et al. (2017). Friction mediates scission of tubular membranes scaffolded by BAR Proteins. *Cell* **170**, 172-184.e11. doi:10.1016/j.cell.2017.05.047

Sinha, B., Köster, D., Ruez, R., Gonnord, P., Bastiani, M., Abankwa, D., Stan, R. V., Butler-Browne, G., Vedie, B., Johannes, L. et al. (2011). Cells respond to mechanical stress by rapid disassembly of caveolae. *Cell* **144**, 402-413. doi:10.1016/j.cell.2010.12.031

Smart, E. J., Graf, G. A., McNiven, M. A., Sessa, W. C., Engelman, J. A., Scherer, P. E., Okamoto, T. and Lisanti, M. P. (1999). Caveolins, liquid-ordered domains, and signal transduction. *Mol. Cell. Biol.* **19**, 7289-7304. doi:10.1128/MCB.19.11.7289

Suetsugu, S., Kurisu, S. and Takenawa, T. (2014). Dynamic shaping of cellular membranes by phospholipids and membrane-deforming proteins. *Physiol. Rev.* **94**, 1219-1248. doi:10.1152/physrev.00040.2013

Tachikawa, M., Morone, N., Senju, Y., Sugiura, T., Hanawa-Suetsugu, K., Mochizuki, A. and Suetsugu, S. (2017). Measurement of caveolin-1 densities in the cell membrane for quantification of caveolar deformation after exposure to hypotonic membrane tension. *Sci. Rep.* **7**, 7794. doi:10.1038/s41598-017-08259-5

Vamparys, L., Gautier, R., Vanni, S., Bennett, W. F., Tieleman, D. P., Antonny, B., Etchebest, C. and Fuchs, P. F. (2013). Conical lipids in flat bilayers induce packing defects similar to that induced by positive curvature. *Biophys. J.* **104**, 585-593. doi:10.1016/j.bpj.2012.11.3836

van Meer, G., Voelker, D. R. and Feigenson, G. W. (2008). Membrane lipids: where they are and how they behave. *Nat. Rev. Mol. Cell Biol.* **9**, 112-124. doi:10.1038/nrm2330

Wang, Q., Navarro, M. V. A. S., Peng, G., Molinelli, E., Lin Goh, S., Judson, B. L., Rajashankar, K. R. and Sondermann, H. (2009). Molecular mechanism of membrane constriction and tubulation mediated by the F-BAR protein Pacsin/syndapin. *Proc. Natl. Acad. Sci. USA* **106**, 12700-12705. doi:10.1073/pnas.0902974106

Wu, E. L., Cheng, X., Jo, S., Rui, H., Song, K. C., Dávila-Contreras, E. M., Qi, Y. F., Lee, J. M., Monje-Galvan, V., Venable, R. M. et al. (2014). CHARMM-GUI membrane builder toward realistic biological membrane simulations. *J. Comput. Chem.* **35**, 1997-2004. doi:10.1002/jcc.23702

Yang, Y., Lee, M. and Fairn, G. D. (2018). Phospholipid subcellular localization and dynamics. *J. Biol. Chem.* **293**, 6230-6240. doi:10.1074/jbc.R117.000582

Zidovetzki, R. and Levitan, I. (2007). Use of cyclodextrins to manipulate plasma membrane cholesterol content: evidence, misconceptions and control strategies. *Biochim. Biophys. Acta* **1768**, 1311-1324. doi:10.1016/j.bbamem.2007.03.026

Figure S1

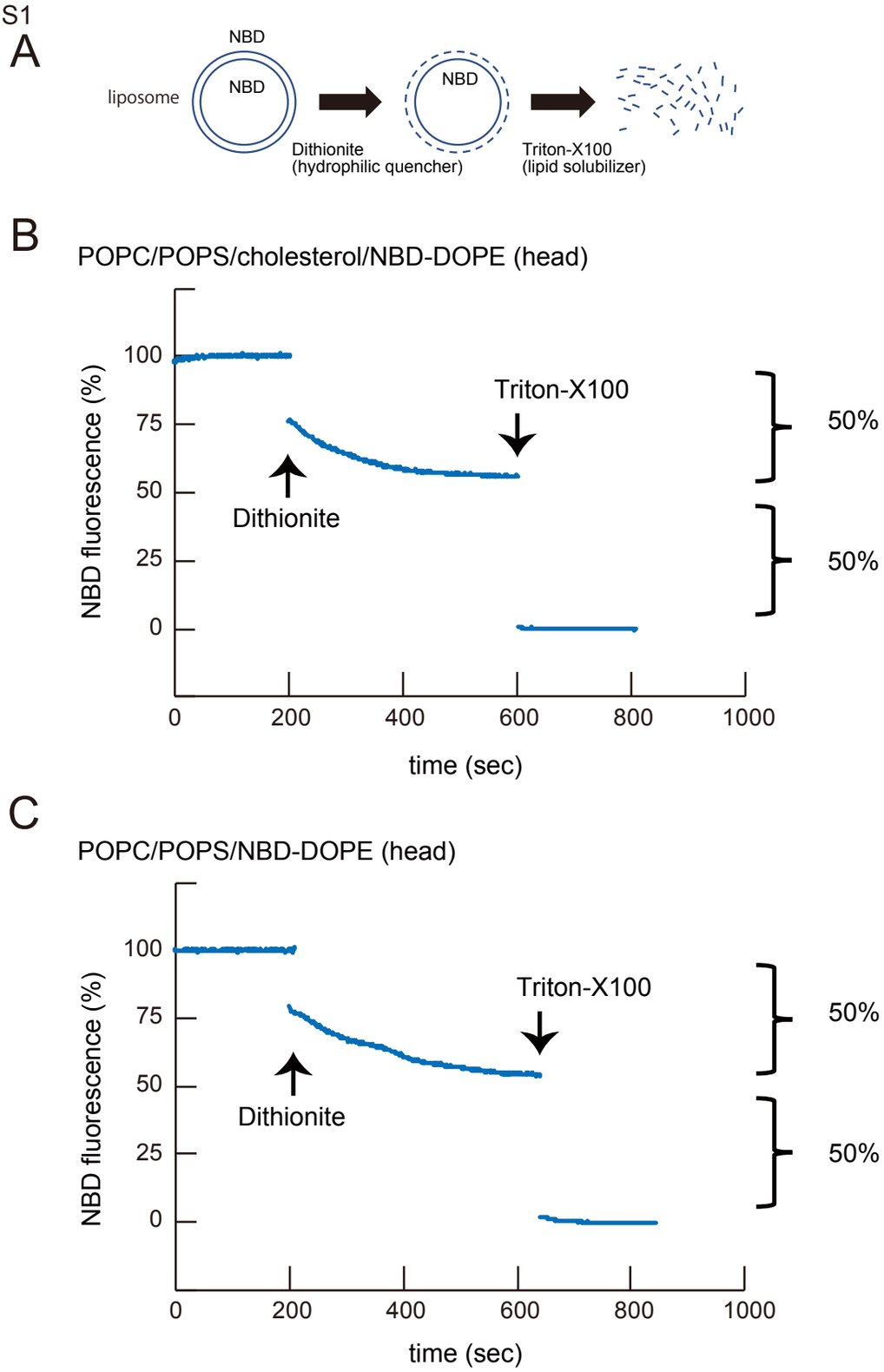

Figure S1. The estimation of lamellarity of liposomal membranes by quenching.

(A) The schematic illustration of the quenching of NBD-labelled lipids in liposome. Both outer and inner leaflets of liposomal membranes contained NBD-labelled DOPE. The hydrophilic quencher Dithionite is impermeable to membrane. Dithionite quenched the NBD at the head of DOPE at the outer leaflet of liposome in the absence of Triton-X 100. After the quenching of NBD on the outer leaflet, the Triton-X 100 was added to solubilize the liposomes, which enabled Dithionite to quench NBD that was located at the inner leaflet of liposome.

(B and C) The time-course of NBD quenching. The liposomes composed of POPC/POPS/cholesterol/NBD-DOPE (33 / 22 / 45 / 1) (B) and POPC/POPS/NBD-DOPE (60 / 40 / 1) (C) were quenched by Dithionite, then followed by the addition of Triton-X 100.

Figure S2

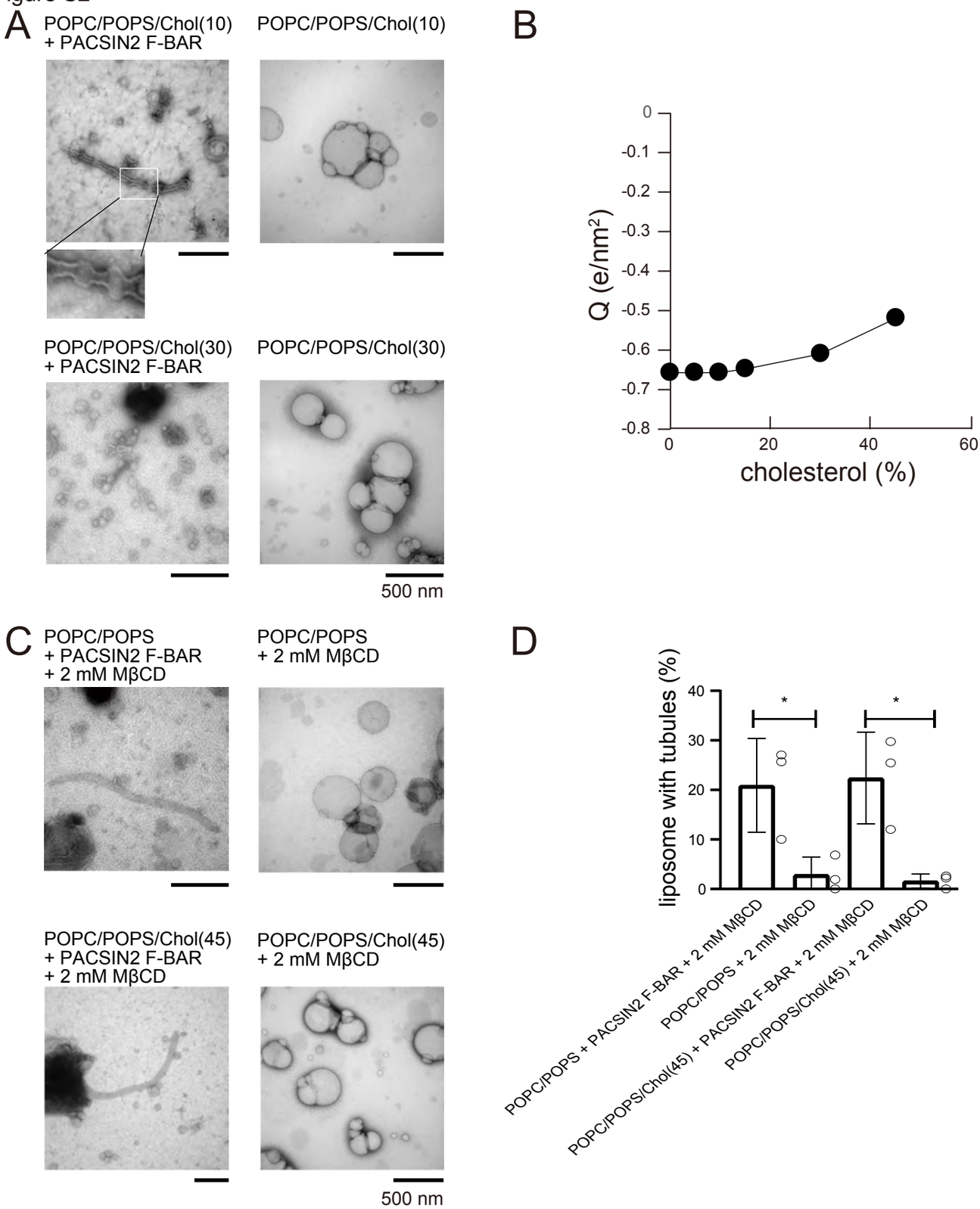

Figure S2. The cholesterol dependency of tubule formation by PACSIN2 F-BAR domain in vitro.
(A) Electron microscopic images of negatively stained liposomes. The liposomes of POPC/POPS/Chol(10) and POPC/POPS/Chol(30) in the presence or absence of PACSIN2 F-BAR domain (5 μM). Liposome concentration, 0.125, 0.1375, and 0.1625 μg/μl, respectively, to have the same amount of POPS.
(B) Molecular dynamics simulation for the estimation of model membrane parameters. The charge density (electron/nm^2) was plotted against the percentage of cholesterol.
(C) Electron microscopic images of negatively stained liposomes. The liposomes of POPC/POPS and POPC/POPS/Chol(45) in the presence or absence of PACSIN2 F-BAR domain (5 μM) in the presence of 2 mM MβCD. Liposome concentration, 0.125 μg/μl.
(D) The quantification of the liposomes with tubules in (A). N= 3. * shows the statistical significance ($p < 0.05$ by a one-way ANOVA followed by Tukey's post hoc test).